RESEARCH ARTICLE

LocZ Is a New Cell Division Protein Involved in Proper Septum Placement in *Streptococcus pneumoniae*

Nela Holečková,[a] Linda Doubravová,[a] Orietta Massidda,[b] Virginie Molle,[c] Karolína Buriánková,[a] Oldřich Benada,[a] Olga Kofroňová,[a] Aleš Ulrych,[a] Pavel Branny[a]

Cell and Molecular Microbiology Division, Institute of Microbiology, v.v.i., Academy of Sciences of the Czech Republic, Prague, Czech Republic[a]; Dipartimento di Scienze Chirurgiche, Sez. di Anatomia Patologica e Microbiologia, Università di Cagliari, Cagliari, Italy[b]; Laboratoire de Dynamique des Interactions Membranaires Normales et Pathologiques, Universités de Montpellier II et I, CNRS, Montpellier, France[c]

ABSTRACT **How bacteria control proper septum placement at midcell, to guarantee the generation of identical daughter cells, is still largely unknown. Although different systems involved in the selection of the division site have been described in selected species, these do not appear to be widely conserved. Here, we report that LocZ (Spr0334), a newly identified cell division protein, is involved in proper septum placement in *Streptococcus pneumoniae*. We show that *locZ* is not essential but that its deletion results in cell division defects and shape deformation, causing cells to divide asymmetrically and generate unequally sized, occasionally anucleated, daughter cells. LocZ has a unique localization profile. It arrives early at midcell, before FtsZ and FtsA, and leaves the septum early, apparently moving along with the equatorial rings that mark the future division sites. Consistently, cells lacking LocZ also show misplacement of the Z-ring, suggesting that it could act as a positive regulator to determine septum placement. LocZ was identified as a substrate of the Ser/Thr protein kinase StkP, which regulates cell division in *S. pneumoniae*. Interestingly, homologues of LocZ are found only in streptococci, lactococci, and enterococci, indicating that this close phylogenetically related group of bacteria evolved a specific solution to spatially regulate cell division.**

IMPORTANCE **Bacterial cell division is a highly ordered process regulated in time and space. Recently, we reported that the Ser/Thr protein kinase StkP regulates cell division in *Streptococcus pneumoniae*, through phosphorylation of several key proteins. Here, we characterized one of the StkP substrates, Spr0334, which we named LocZ. We show that LocZ is a new cell division protein important for proper septum placement and likely functions as a marker of the cell division site. Consistently, LocZ supports proper Z-ring positioning at midcell. LocZ is conserved only among streptococci, lactococci, and enterococci, which lack homologues of the Min and nucleoid occlusion effectors, indicating that these bacteria adapted a unique mechanism to find their middle, reflecting their specific shape and symmetry.**

Received 24 July 2014 **Accepted** 1 December 2014 **Published** 30 December 2014

Citation Holečková N, Doubravová L, Massidda O, Molle V, Buriánková K, Benada O, Kofroňová O, Ulrych A, Branny P. 2015. LocZ is a new cell division protein involved in proper septum placement in *Streptococcus pneumoniae*. mBio 6(1):e01700-14. doi:10.1128/mBio.01700-14.

Invited Editor Kevin D. Young, University of Arkansas for Medical Sciences **Editor** Larry S. McDaniel, University of Mississippi Medical Center

Address correspondence to Linda Doubravová, linda@biomed.cas.cz, or Orietta Massidda, omassid@unica.it.

Bacterial cell division begins with the polymerization of the tubulin-like FtsZ protein that forms a ring (the Z-ring) at the division site (1), precisely located at the middle of the cell. The mechanism is so accurate that daughter cells vary very little in size (2). Proper localization and polymerization of FtsZ are required to guarantee the production of two identical daughter cells, as well as to recruit the downstream cell division proteins that, together with FtsZ, form the cell division machinery, the divisome (3–6).

While some of the events that follow the localization of FtsZ are fairly well understood and many proteins that participate in the cell division process have been recognized and are conserved among the different bacteria, those that spatially and/or temporally regulate correct positioning of FtsZ are generally not conserved (7, 8). As a consequence, how FtsZ finds the middle of the cell in many species is yet an unsolved question.

In the model rod-shaped organisms *Escherichia coli* and *Bacillus subtilis*, precise positioning of the Z-ring at the cell center is achieved by the action of two systems, the nucleoid occlusion (NO) and the Min system (8–11), which prevent FtsZ from assembling anywhere else other than at midcell. The former mechanism is mediated by SlmA in *E. coli* (12–15) and Noc in *B. subtilis* (16, 17). These nonhomologous proteins negatively affect FtsZ polymerization (13, 14, 18) until chromosome segregation relieves the block, allowing the Z-ring to form. The Min system (19–22) spatially regulates cell division, by preventing the Z-ring from assembling at inappropriate noncentral sites, through inhibition of FtsZ polymerization (23, 24). In the absence of the inhibitory Min proteins, *E. coli* and *B. subtilis* cells divide also at or near the cell poles, generating DNA-less minicells (25, 26). Some bacterial species have only one of the two systems described above, while many others lack both the Noc/SlmA and the Min protein homologues (7, 8, 27), suggesting that other mechanisms for correct septum placement should exist. For example, MipZ, a protein conserved in all alphaproteobacteria that lack the Min homologues, has been

found to inhibit Z-ring assembly in *Caulobacter crescentus* (28), while another protein, PomZ, was recently found required to position the cell division site in *Myxococcus xanthus* (29).

Streptococcus pneumoniae is an oval Gram-positive coccus that, similarly to the rod-shaped model organisms, divides in parallel planes perpendicular to its long axis (30–32). During the cell cycle, *S. pneumoniae* achieves and maintains its oval cell shape by alternating peripheral peptidoglycan (PG) synthesis, which occurs during cell elongation, with septal PG synthesis, which occurs during cell division, although the latter prevails over the former (33, 34). The cell division site is marked by a "wall band" or "equatorial ring" at the largest cell diameter. Soon after division starts, the equatorial ring is split into two identical rings, which delimit a central zone for peripheral PG synthesis and progressively move away from the center to become the cell division markers in the newly generated daughter cells (30, 35). Although no mechanism for targeting the division machinery to the nascent septum has been identified in *S. pneumoniae* and the precise order of recruitment of the cell division proteins to the divisome is yet to be determined, the essential cell division initiator proteins FtsZ and FtsA localize to midcell at the earliest stages of the process (36, 37). This event is then followed by the localization of the cell division regulator protein StkP (38) and the later cell division proteins DivIB (FtsQ), DivIC (FtsB), FtsL, FtsW, PBP2x, and PBP1a (37, 39, 40) and DivIVA (41), which localize only after the FtsZ-ring has assembled.

Here we report, for the first time, the identification of LocZ (for *Loc*alizing at midcell of Fts*Z*), a topological determinant for cell division in *S. pneumoniae*. Our data show that LocZ arrives at midcell before FtsZ and FtsA, and its activity is important for proper septum placement, cell shape, and division. Based on its localization pattern and null mutant phenotype, LocZ is a putative marker to recruit FtsZ to midcell, likely acting as a positive regulator of Z-ring formation.

RESULTS

Inactivation of *locZ* in *S. pneumoniae*. We previously identified Spr0334 (now named LocZ) as one of the substrates phosphorylated, both *in vitro* and *in vivo*, by the eukaryotic-like kinase Ser/Thr kinase, StkP (42). LocZ is a membrane protein of unknown function. It consists of a predicted cytoplasmic domain (amino acids [aa] 1 to 158), a putative transmembrane domain (aa 159 to 179), and an extracellular part (aa 180 to 464) (Fig. 1A; see also Fig. S1 in the supplemental material). Sequence comparison showed that LocZ is present only in streptococci, lactococci, and enterococci and that it is not homologous to any other known protein and does not contain any annotated conserved domains, even when the most conserved N- and C-terminal regions were analyzed separately.

To assess the function of LocZ, we prepared a nonpolar markerless mutant, using a Cheshire cassette for gene inactivation in *S. pneumoniae* (43). The resulting Δ*locZ* strain was named Sp57. Deletion of *locZ* was confirmed by immunoblotting with anti-LocZ polyclonal antibodies (Fig. 1B), which documented the presence of LocZ in the wild type (WT) and its absence in the Sp57 null mutant. Consistent with the fact that LocZ is phosphorylated on Thr residues *in vivo* (42), immunodetection with anti-phospho-Thr (anti-pThr) antibodies revealed a phosphorylated protein of the size of LocZ in the cell lysates of the WT strain but not in those of the Sp57 null mutant (Fig. 1B). To exclude the possibility of a polar effect due to *locZ* deletion, analysis of the transcription level of adjacent genes was performed by quantitative reverse transcription PCR (qRT-PCR). No changes in the expression of the flanking *spr0332*, *spr0333*, *spr0335*, and *spr0336* genes were observed (see Table S1 in the supplemental material), indicating that deletion of *locZ* did not prevent the expression of the upstream or the downstream genes in the operon. A polar effect was further ruled out by complementation experiments (see below).

Sp57 showed a doubling time and viability similar to those of the WT strain (Fig. 1C), although the lag phase was somewhat longer. As StkP is important for competence for genetic transformation and resistance to heat and oxidative and osmotic stresses and acid tolerance (44), we tested if its substrate LocZ also played a role in stress tolerance. The *locZ* null mutant was more sensitive to heat stress than the WT (Fig. 1D) and showed 50% lower survival after exposure to oxidative stress (10 mM H_2O_2) (data not shown). However, we did not observe significant differences in the sensitivity of Sp57 to osmotic stress and to low pH value and competence for genetic transformation (data not shown), suggesting that stress resistance is not generally regulated through phosphorylation of LocZ via StkP.

Absence of LocZ results in septum misplacement and cell division defects. Since StkP regulates cell division in *S. pneumoniae* (38), we then examined the morphology of the Sp57 null mutant by both phase-contrast and electron microscopy. Albeit viable, the Δ*locZ* mutant showed severe cell division defects, with cells dividing asymmetrically, generating daughter cells of unequal size (Fig. 1F, 2, and 3; Table 1). As a consequence, abnormally small cells, resembling minicells, were frequently observed (Fig. 1F, 2, and 3; Table 1). Analysis of phase-contrast images revealed that 31.8% (127/400) of the cells in strain Sp57 divided asymmetrically. Measuring the cell length with the automated MicrobeTracker software (45), we found that cells lacking LocZ were significantly shorter (1.61 $\pm$ 0.39 μm in strain Sp57) than the WT cells (1.83 $\pm$ 0.39 μm; $P \leq 0.0001$, Mann-Whitney rank sum test) (Table 1), and their distribution in distinct length classes significantly differed from that of the WT (Fig. 1E). To quantify the number of minicells, we then defined the length of the smallest WT cell as the minimal normal cell length and determined that 5.5% (22/400) of the Sp57 mutant cells were smaller. Interestingly, DAPI (4′,6-diamidino-2-phenylindole) staining showed that 2.5% (10/400) of cells of the whole population, accounting for 45% of the smaller cells (i.e., cells with lengths of $\leq$1 μm), lacked DNA and thus were true minicells (Fig. 1F), which were not previously described in *S. pneumoniae*. These minicells were always paired with larger cells, which contained DNA.

Scanning electron microscopy confirmed phase-microscopy findings and provided a more detailed picture (Fig. 2). Wild-type cells at different stages of the cell cycle displayed the characteristic oval morphology (Fig. 2A). On the other hand, 75% of the mutant cells looked misshapen (Fig. 2B), had unequal daughter cell size, and produced minicells. Moreover, many cells, independently of their length, showed an irregular "potato-like" shape and abnormal poles, as the result of division septa placed not perpendicular to the long axis of the cell. Occasionally, cells with more than one incipient septum were also observed (Fig. 2B, subpanel B5). Transmission electron microscopy (TEM) revealed that some cells contained two invaginations, due to the presence of double partial septa in close proximity (Fig. 3C) and other cells that contained two septa at different stages of closure (Fig. 3D). Nevertheless,

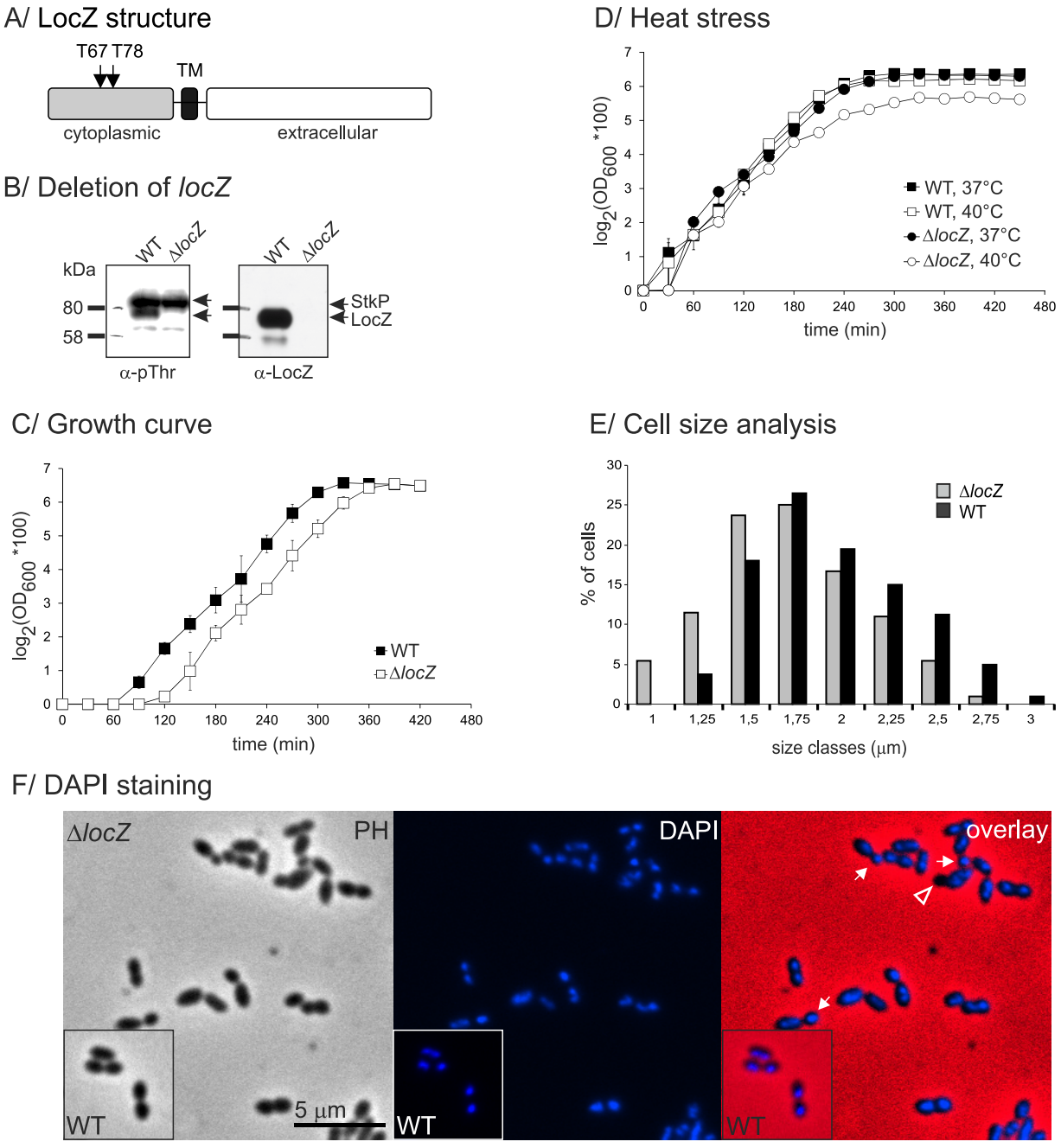

FIG 1 LocZ domain organization and mutant analysis. (A) Domains of LocZ. LocZ is composed of an N-terminal cytoplasmic domain, a single transmembrane (TM) region, and a C-terminal extracellular part. The two phosphoacceptor threonine residues in the cytoplasmic domain are indicated. (B) Deletion of *locZ*. Detection of LocZ in whole-cell lysates of the WT (Sp1) and the Δ*locZ* (Sp57) strains with anti-LocZ (α-LocZ) polyclonal antibodies. Phosphorylation was verified with anti-pThr (α-pThr) antibodies. (C) Growth characteristics of Rx1 wild type (Sp1) and Δ*locZ* mutant (Sp57). Strains were grown in TSB medium at 37°C. Turbidity of the culture was monitored at OD_{600} every 30 min. Doubling times were 35 min for both strains. (D) Sensitivity to heat stress. Sp1 and Sp57 strains were cultivated in TSB at 37°C or 40°C, and growth was monitored as described for panel C. The standard errors of the means of three independent experiments are shown. (E) Cell length analysis. The histogram shows the distribution of cells of the WT (Sp1) (black) and Δ*locZ* mutant (Sp57) (gray) in distinct size classes. Numbers on the *x* axis indicate the size of the longest cell in the corresponding class. (F) Morphology of Δ*locZ* mutant. WT (Sp1) and Δ*locZ* (Sp57) cells were fixed, stained with DAPI, and examined by phase-contrast and fluorescent microscopy. White arrows indicate abnormally small cells generated by the asymmetric division of strain Sp57. The white arrowhead indicates those small cells (minicells) that do not contain DNA. PH, phase contrast; DAPI, DNA; overlay, overlay of PH and DAPI. Bar, 5 μm.

despite these abnormalities, there were many cells with completed septa.

Given the cell division defects described above, we examined the nascent sites of peptidoglycan (PG) biosynthesis by use of fluorescent vancomycin (VanFL) (46). VanFL staining of the WT strain resulted in a typical pattern in which cell wall synthesis was

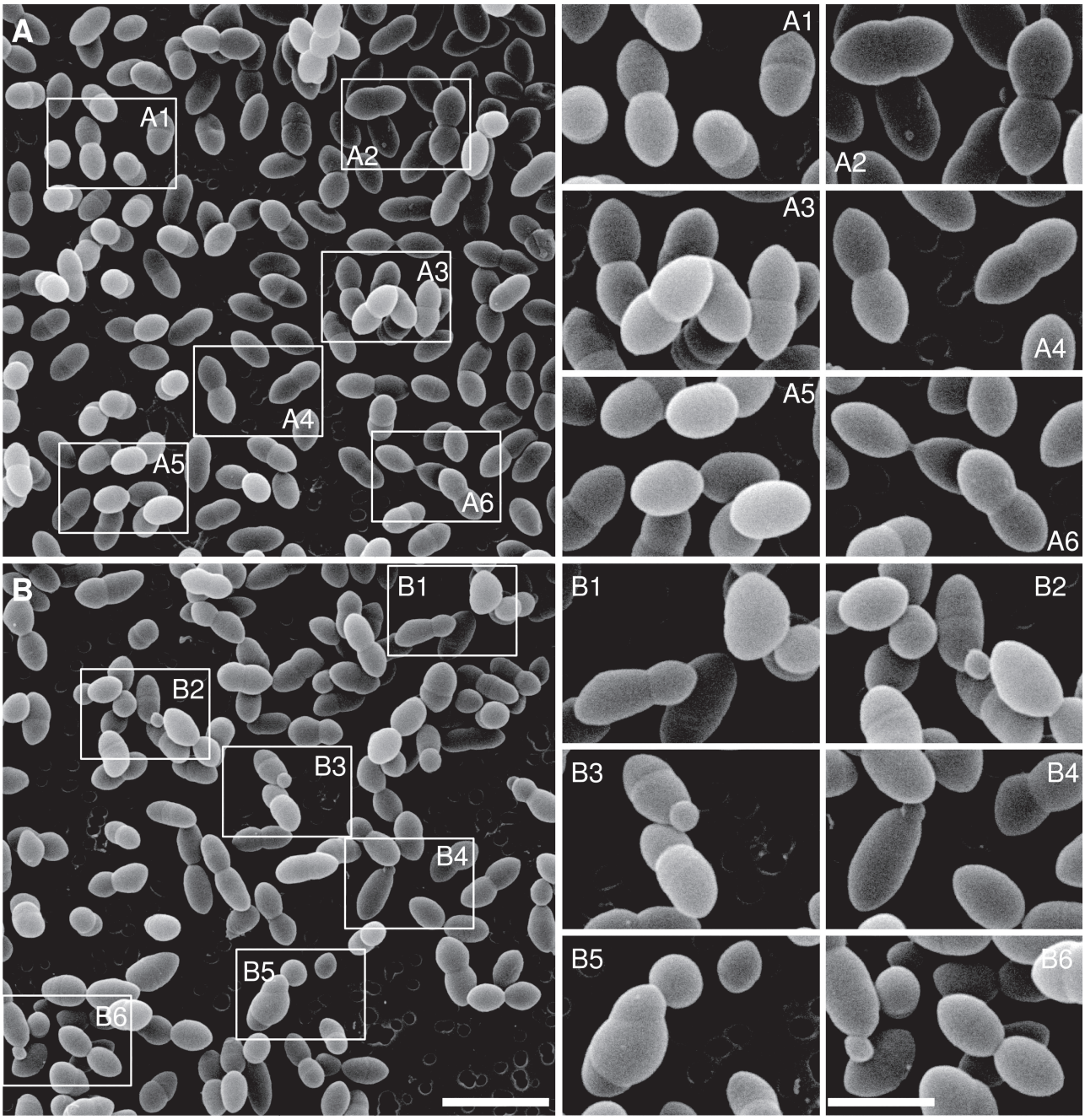

FIG 2 Scanning electron microscopy of Δ*locZ* mutant (Sp57) and wild-type *S. pneumoniae* (Sp1) cells. (A and B) Overviews of the WT (A) and the Δ*locZ* mutant (B). The boxes indicate the areas shown in the panels on the right. In panels A1 to A6, WT cells with the characteristic diplococcal morphology, including individual cells (A5) or cells at different stages of cell division (A1 to A4 and A6), can be seen. Dividing cells are similar in shape and size, with septa perpendicular to the long cell axis. In panels B1 to B6, altered morphology of the Δ*locZ* mutant is presented. Panel B1 shows that Sp57 dividing cells are uneven in shape and size. The cell poles are deviated from the long cell axis. A typical potato-like cell is shown in the upper right corner. In panels B2 to B4 and B6, typical minicells can be seen at one of the cell poles. B5 shows an unusual cell with two septa not perpendicular to the long cell axis. The magnifications of the images in panels A and B are the same. Bar, 2 μm. The images in panels on the right are magnified twice. Bar, 1 μm.

labeled at midcell and at the equators of future daughter cells (see Fig. S2A in the supplemental material). On the other hand, although synthesis was also detected at the current division sites in the Δ*locZ* mutant cell wall, in many cells septa were clearly shifted from the center and/or not perpendicular to the longitudinal axis of the cell (Fig. S2A). Moreover, VanFL labeling at the equators of daughter cells was not so evident in the Sp57 mutant. Few cells of abnormal shape showed fuzzy fluorescent signals, not restricted to a particular area (open arrow in Fig. S2). These findings reflect the cell morphology observed by phase-contrast and electron microscopy, suggesting that LocZ may be a new cell division component involved in proper septum placement.

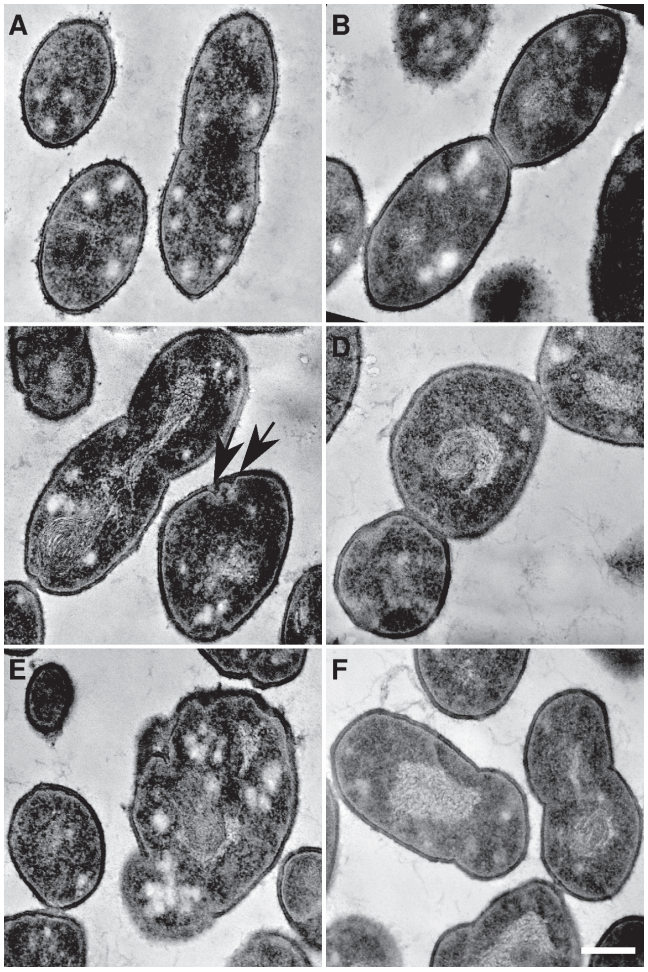

FIG 3 Transmission electron microscopy of Δ*locZ* mutant (Sp57) and wild-type *S. pneumoniae* (Sp1) cells. (A and B) Typical cell division of WT strain. (A) Beginning of septum formation. (B) Cells with well-developed septum, just before their separation. (C to F) Altered ultrastructure of the Δ*locZ* mutant. (C) Example of the configuration of several septa; invaginations in close proximity are marked by arrows. (D) Example of three cells still connected by the septa. (E) Example of bacterial cell lysis; the cell wall rupture and altered cytoplasm can be seen. (F) Uneven cell division resembling the cells shown in Fig. 2B, subpanel B1. Magnifications are the same for all images. Bar, 0.2 μm.

Mutations or deletion of cell division genes in *S. pneumoniae* may show a strain-dependent phenotype (33). Therefore, to ensure that the Δ*locZ* phenotype did not depend on the genetic background, we constructed a nonpolar markerless mutant also in the unencapsulated R6 strain and in the encapsulated D39 progenitor. The resulting strains, Sp239 (R6; Δ*locZ*) and Sp267 (D39; Δ*locZ*), respectively, showed a phenotype indistinguishable from that of Sp57 (see Fig. S2B in the supplemental material), confirming that lack of LocZ results in the same cell division defects in different genetic backgrounds.

Complementation of Δ*locZ* restores the wild-type phenotype. To confirm that the observed phenotype was caused by the deletion of *locZ*, we constructed a strain (Δ*locZ bga*::P_{czcD}-*his6-locZ*) named Sp60, carrying a histidine-tagged *locZ* wild-type allele under the control of the zinc-inducible P_{czcD} promoter (47), as the only source of *locZ* in the chromosome. Sp60 cells, cultured in the absence of the inducer Zn^{2+}, did not express LocZ and showed morphology, size, DAPI staining pattern, and growth characteristics similar to those of the *locZ* null mutant (Table 1; also see Fig. S3A, C, and D in the supplemental material). When grown in the presence of Zn^{2+}, Sp60 cells expressed His6-LocZ, albeit at a lower level than LocZ in the WT (Fig. S3B), but nonetheless sufficient to fully restore WT morphology and size (Table 1; see also Fig. S3A, C, and D).

LocZ localizes to midcell during cell division. The *locZ* null mutant phenotype suggested that the protein could play a role in cell division. Therefore, we determined its localization in exponentially growing cells using LocZ tagged to the green fluorescent protein (GFP), in the Sp229 strain, which expresses *gfp-locZ* from its chromosomal locus under the control of its native promoter as the only copy of LocZ. The GFP-LocZ fusion was functional, because the Sp229 strain was indistinguishable from the WT (Fig. 4; see also Fig. S4A in the supplemental material).

As expected for a cell division protein, LocZ localized to midcell during the cell cycle. However, a more detailed analysis of the conventional six stages of pneumococcal cell division (41) revealed a unique localization profile of GFP-LocZ (Fig. 4), so far not observed for other cell division proteins (33). As shown in Fig. 4, in cells at the first stage of cell division, i.e., newborn single oval cells, 2.8% (17/610) of the population, LocZ was already present as a ring at midcell. In cells at stage 2, which had begun elongation, accounting for 27.5% (168/610) of the cells, LocZ formed a striking double band still located in the central position. As elongation proceeded, at stage 3, accounting for 20% (122/610) of the cells, the two LocZ rings progressively separated from each other. At stage 4, when the central invagination indicated the start of septum constriction, accounting for 17.4% (106/610) of the cells, LocZ appeared localized as two rings, at the respective equators of the future daughter cells, where it remained until completion of the current cell division (stage 5) and separation (stage 6), accounting, respectively, for 16.9% (103/610) and 15.4% (94/610) of the population.

We then examined the localization of GFP-LocZ in the Δ*stkP*

TABLE 1 Descriptive statistics of cell size[a]

Strain	Zn^{2+}	Min	First quartile	Median	Third quartile	Max	Mean	SD	Width	Asymmetric division (%)	Minicells (%)	Anucleate cells (%)
Sp1	−	1.00	1.53	1.77	2.08	2.81	1.83	0.39	0.67	0.00	0.00	0
Sp57	−	0.66	1.34	1.59	1.88	2.66	1.61	0.39	0.66	31.80	5.50	2.5
Sp60	−	0.63	1.29	1.55	1.83	3.01	1.57	0.44	0.65	29.00	10.25	2.7
Sp60	+	1.04	1.47	1.67	1.97	2.78	1.75	0.36	0.67	0.75	0.00	0

[a] Cell size (μm) of 400 cells in each strain was measured using automated MicrobeTracker software, and cell length results were analyzed by GraphPad Prism 3.0 (columns 3 to 10). Min, minimum; Max, maximum; SD, standard deviation; Zn^{2+}, strain was cultivated in the presence of 0.45 mM $ZnCl_2$ to induce expression of His6-LocZ. The number of asymmetrically dividing cells was evaluated from phase-contrast microscopic pictures. Minicells represent all cells shorter than 1 μm (the minimal length of WT cells).

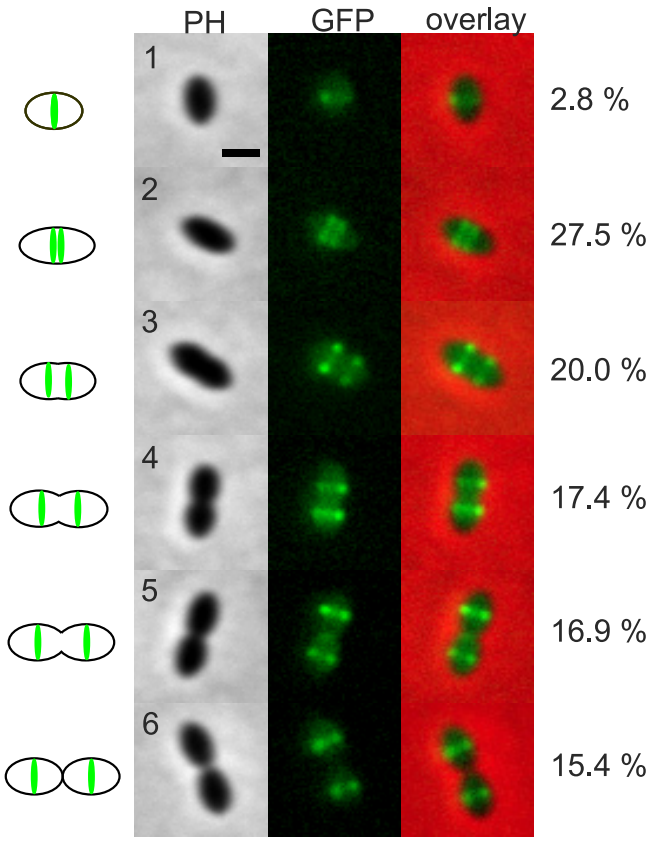

FIG 4 Localization of GFP-LocZ in *S. pneumoniae*. A representative cell for each conventional stage of the pneumococcal cell cycle (designated 1 to 6) illustrates the localization of GFP-LocZ expressed under the control of its native promoter (strain Sp229). Phase contrast (PH), GFP signal (GFP), and overlays are shown. Schematic pictures on the left document the position of the GFP signal in the cells. The percentages of cells at each stage over 610 cells are shown on the right. All cells at each stage showed the same localization profile as did the representative cell shown in the figure. Bar, 1 μm.

genetic background. For this purpose, we constructed a Δ*stkP* strain (Sp58; Δ*stkP bga*::P_{czcD}-*gfp-locZ*), expressing *gfp-locZ* under the control of the P_{czcD} inducible promoter. Δ*stkP* mutant cells (see Fig. S4B in the supplemental material) displayed a characteristic elongated morphology (42) with multiple Z-rings (38) and failed to phosphorylate LocZ (42). In these cells, Zn^{2+}-induced GFP-LocZ localized to multiple division septa, in a pattern similar to the localization previously reported for FtsA and DivIVA (38). Hence, targeting of LocZ to midcell precedes StkP and does not depend on StkP and/or its phosphorylation state.

LocZ is an early component of the pneumococcal cell division machinery. The above data suggested that LocZ may be an early cell division protein. Therefore, we determined the dynamics of LocZ localization and the timing of its arrival at midcell relative to FtsZ and FtsA, which are the earliest proteins known to localize at the division site in *S. pneumoniae* (36, 37). For this purpose, we constructed strains allowing the simultaneous expression and visualization of LocZ and FtsZ or FtsA, fused to different fluorescent tags. The resulting double-labeled Sp242 (*rfp-locZ*, pBCSMH036) and Sp256 (*rfp-locZ*, *bgaA*::P_{czcD}-*gfp-ftsA*) strains express red fluorescent protein (RFP)-LocZ under the control of its native promoter and, respectively, cyan fluorescent protein (CFP)-FtsZ from a plasmid under the control of a constitutive promoter (48) or GFP-FtsA under the control of the P_{czcD} inducible promoter (38).

We analyzed then the cellular localization of the coexpressed fusion proteins at the six stages of pneumococcal cell division (Fig. 5; also see Fig. S4E in the supplemental material). As shown in Fig. 5, LocZ and FtsZ (Fig. 5A) or LocZ and FtsA (Fig. 5B) colocalize in cells at the predivisional stage 1, accounting for 7.8% (28/359) and 12% (47/389) of the cells, respectively. Soon after cell division starts, and the cells undergo the initial elongation (stage 2), LocZ splits into two bands that, as elongation proceeds, progressively move away from the center (stage 3). At these stages, CFP-FtsZ and GFP-FtsA are still detected as a ring at midcell, 19.5% (72/359) and 23.1% (83/389) and 20% (72/359) and 21.3% (83/389) of cells, respectively. This is best appreciated in the fluorescence intensity profiles of cells at stages 2 and 3, showing the RFP-LocZ signal separated into two peaks, while the CFP-FtsZ and GFP-FtsA signals are in a single midcell peak. As cell division progresses, an observable Z-ring constriction at the current division site coincides with new FtsZ and FtsA rings formed at the future division sites, occupied by LocZ (stage 4), 15.8% (57/359) and 17.7% (69/389) of cells, respectively. Consistently, the fluorescence intensity profiles corresponding to FtsZ and FtsA form a triple peak, with maxima at the center of the cells and two local maxima overlapping with RFP-LocZ peaks at the new equators. The relocalization of FtsZ and FtsA is even more evident at stage 5, where a complete overlap of the fluorescent signals at the equators of the daughter cells, i.e., the future division sites, 16.4% (59/359) and 12.1% (47/389) of the cells, respectively, is observed. Finally, in cells at stage 6, 20.3% (73/359) and 13.6% (53/389) of cells, which have completed cell division and represent newly born daughter cells, RFP-LocZ and CFP-FtsZ or GFP-FtsA, respectively, are again colocalized at midcell. These data indicate that LocZ arrives and leaves the midcell early, before FtsZ and FtsA, and that its position overlaps with the equators of the cell, which mark the sites for the next division.

The picture above was even more striking when we determined the localization of the protein kinase StkP and its substrate LocZ in the Sp248 (*rfp-locZ bga*::P_{czcD}-*gfp-stkP*) strain, which expresses RFP-LocZ from its native promoter and GFP-StkP under the control of the P_{czcD} promoter (Fig. 5C; also see Fig. S4E in the supplemental material) (38). As expected, GFP-StkP was enriched at midcell, associated with the FtsZ-ring, until signs of constriction were visible and relocalized at the new equators later than FtsZ and FtsA (38), while RFP-LocZ localized to the midcell only at the initial stages of the process. These results show that LocZ and StkP colocalize mainly at the early stage of cell division, in single oval cells at stage 1, accounting for 9% of cells (32/354), and in newly born cells at stage 6, which have already divided but not yet separated, accounting for 18.9% (67/354) of the cells, suggesting that the predivisional stage is the most likely phase at which LocZ can be phosphorylated by StkP.

FtsZ and FtsA are mislocalized in Δ*locZ* mutants. The morphological abnormalities of the Δ*locZ* null mutant indicated that the observed asymmetric cell division defects may be caused by a misplacement of the Z-rings. To test this, we constructed strain Sp243 (Δ*locZ*, pBCSMH036), constitutively expressing CFP-FtsZ (48), and strain Sp257 (Δ*locZ bga*::P_{czcD}-*gfp-ftsA*), expressing inducible GFP-FtsA (38), and monitored FtsZ and FtsA localization throughout the cell cycle by time-lapse fluorescence microscopy

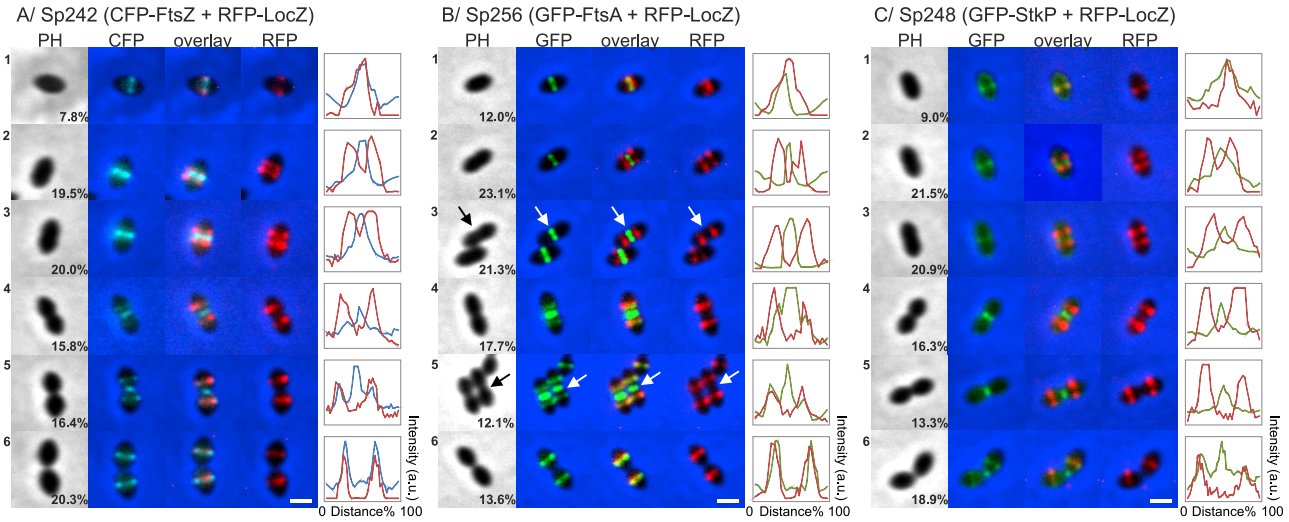

FIG 5 Colocalization of LocZ and FtsZ, FtsA, or StkP. Double-labeled strains, expressing RFP-LocZ at the native locus from its native promoter and CFP-FtsZ, GFP-FtsA, or GFP-StkP from the constitutive or P_{czcD} promoter, analyzed by fluorescence microscopy. Cells representing the six different stages of *S. pneumoniae* cell division are shown. The percentages of cells in each division stage, over 359, 389, and 354 cells counted, respectively, are indicated in the PH panel. All cells at each stage showed the same localization profile as that of the representative cell shown in the respective figure. (A) Sp242 (*rfp-locZ*, pBCSMH036) expresses CFP-FtsZ under the control of the constitutive promoter on the plasmid. (B) Sp256 (*rfp-locZ bgaA*::P_{czcD}-*gfp-ftsA*) expresses GFP-FtsA under the control of the P_{czcD} inducible promoter. (C) Sp248 (*rfp-locZ bgaA*::P_{czcD}-*gfp-stkP*) expresses GFP-StkP under the control of the P_{czcD} inducible promoter. Phase contrast (PH), GFP signal (GFP), CFP signal (CFP), RFP signal (RFP), and corresponding overlays are shown. Bar, 1 μm. Fluorescence intensity profiles of CFP-FtsZ (blue), GFP-FtsA (green), or GFP-StkP (green) versus RFP-LocZ (red) in arbitrary units (a.u.) along the cell length are shown on the right. Arrows indicate the cell analyzed in pictures containing multiple cells.

(Fig. 6; see also Movies S1 and S2 in the supplemental material). Figure 6 shows frames from the corresponding movies, with arrows indicating the different events that occur during cell division. Both FtsZ and FtsA tagged proteins formed a ring structure in Δ*locZ* dividing cells, but frequently these rings were mislocalized (Fig. 6; Movies S1 and S2). Many of the rings were displaced from the cell center and often oriented randomly with respect to the long and the short cell axis, resulting in daughter cells of variable size. Occasionally, two Z-rings were observed in the same cell. Some of the minicells could still divide, while others could not, likely due to lack of DNA (Fig. 6). Interestingly, we also observed abnormally shaped cells containing horseshoe-like CFP-FtsZ structures (Fig. 6A). These cells did not divide but instead increased in volume. Similarly, large and slowly dividing or nondividing cells with horseshoe-like GFP-FtsA structures were observed in strain Sp257 (Fig. 6B). These data indicate that, although LocZ is not strictly required for the Z-ring formation, in its absence the geometric symmetry of the cell is lost and proper positioning of the Z-ring is severely disturbed.

Localization of other cell division proteins in Δ*locZ* mutant. Since localization of FtsZ and FtsA was disturbed in the Δ*locZ* mutant, we also examined the localization of StkP and DivIVA, which are targeted to midcell later than FtsZ and FtsA (38). In the WT Sp246 strain expressing GFP-StkP under the control of the P_{czcD} inducible promoter, StkP localized at the cell membrane with a clear enrichment at the cell division sites (see Fig. S4C in the supplemental material), as previously reported (38). In the mutant strain Sp249 (Δ*locZ bga*::P_{czcD}-*gfp-stkP*), GFP-StkP localized also mainly to the cell division septa, which, however, were often shifted away from midcell (Fig. S4C). From these data, we conclude that LocZ is not required for the localization of StkP, which localizes in the *locZ* null mutant with the rest of the cell division machinery. Similarly, also DivIVA-GFP localized to midcell and cell poles (Fig. S4D) as previously reported (38, 41) in both the WT Sp250 strain and the Sp253 (Δ*locZ bga*::P_{czcD}-*divIVA-gfp*) mutant (Fig. S4D), indicating that LocZ is also not required to target DivIVA to the septum. However, in this case, the characteristic polar dots of DivIVA-GFP helped to illustrate that not only the midcell but also the poles of many cells in the Δ*locZ* mutant deviated from the longitudinal axis. Notably, we observed that in some abnormally shaped cells, DivIVA-GFP formed clusters at atypical positions, indicating an inability to recognize the cell poles (Fig. S4D).

LocZ is phosphorylated on T67 and T78 *in vivo*. To identify the nature and location of the phosphorylation site(s) on LocZ, we used the pETDuet system based on the dual expression of the kinase with its substrate in the surrogate *E. coli* (49). Mass spectrometry analysis unambiguously identified the presence of two phosphate groups, T67 and T78 (Table 2), indicating that LocZ is specifically phosphorylated by StkP.

To confirm phosphorylation of both residues, we replaced them with unphosphorylatable alanine (A) by site-directed mutagenesis to introduce single or double mutations (Thr to Ala). The corresponding LocZ derivatives were expressed and purified as His-tagged proteins in *E. coli*. Following incubation with StkP and [γ-^{32}P]ATP, SDS-PAGE–autoradiography revealed that phosphorylation was partially inhibited in the LocZ-T67A and LocZ-T78A mutants and that this inhibition was almost complete in the doubly mutated LocZ-T67A/T78A protein (Fig. 7A). However, a residual phosphorylation signal of LocZ-T67A/T78A suggested that the doubly mutated protein was still weakly phosphorylated. Since no other phosphoresidues were detected, we mutated also S80, previously identified together with T78 as a phosphoacceptor residue in a global study (50). Nevertheless, phosphoryla-

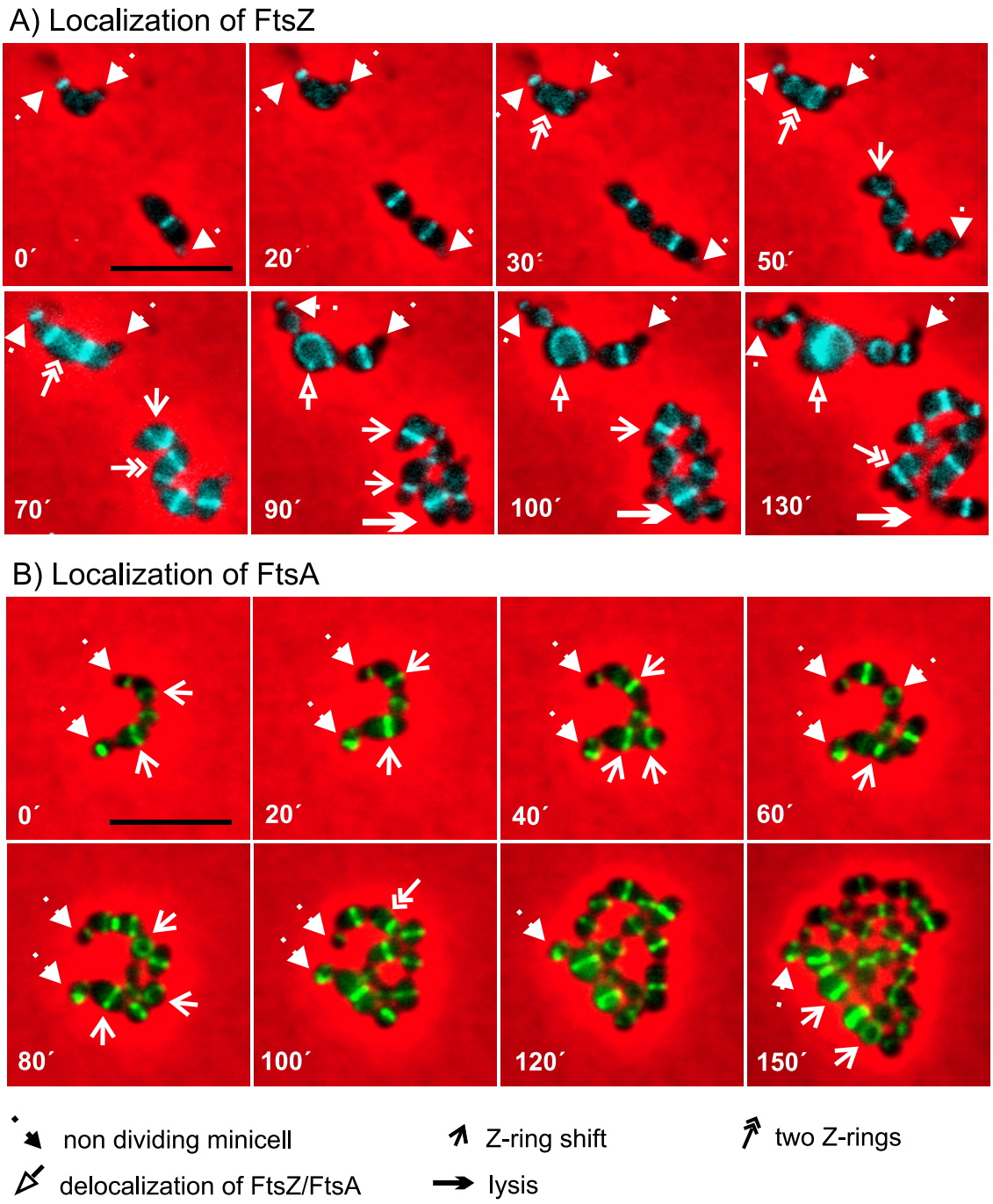

FIG 6 Localization of FtsZ and FtsA in dividing cells of Δ*locZ* mutant strain. Fluorescence time-lapse microscopy of strain Sp243 (Δ*locZ* pBCSMH036) expressing CFP-FtsZ (A) and strain Sp257 (Δ*locZ bga*::P_{czcD}-*gfp-ftsA*) expressing GFP-FtsA (B). Stills are from Movies S1 and S2 in the supplemental material. Representative time points were chosen to illustrate features of Δ*locZ* mutant cell division. Overlays between phase-contrast and fluorescence signals are shown. Five types of arrows (see key at bottom) indicate diverse events in cell division of the mutant: nondividing minicells, shift of the Z-ring from midcell to random position within the cell, occurrence of two Z-rings in one cell, delocalization of FtsZ and loss of ring structure, and cell lysis. Bar, 5 μm.

tion of the triply mutated LocZ-T67A/T78A/S80A protein was comparable to that of the double mutant (Fig. 7A), indicating that there may be a yet-unidentified phosphoacceptor amino acid in LocZ *in vitro*, though its phosphorylation is minimal.

To understand the role of phosphorylation *in vivo*, we constructed strain Sp234 (R6, *locZ*-T67A/T78A) expressing LocZ-T67A/T78A at its native locus under the control of its own promoter. Immunodetection with specific antibodies showed that the level of expression of the unphosphorylated protein was similar to that of the WT (Fig. 7B). Accordingly, the protein did not react with anti-pThr antibodies, confirming that it was not phosphorylated and T67 and T78 are indeed the phosphoacceptors *in vivo*. Nevertheless, phenotypic analysis did not reveal any differences between the *locZ* phosphoablative mutant and the WT strain (data

TABLE 2 Phosphoacceptors identified after purification of *S. pneumoniae* LocZ from the *E. coli* BL21(DE3) Star strain coexpressing StkP[a]

Phosphorylated tryptic peptide sequence of LocZ purified from pCDFDuet coexpressing StkP	No. of phosphate groups detected by LC-MS/MS	Phosphorylated residue
[55–68] QHRDEIEADKFA**pT**R	1	T67
[53–70] VKQHRDEIEADKFA**pT**RQY	1	T67
[71–88] KKEEFVE**pT**QSLDDLIQEM	1	T78

[a] Sequences of the phosphorylated peptides identified in LocZ as determined by liquid chromatography-tandem mass spectrometry (LC-MS/MS) following tryptic digestion are indicated, and phosphorylated residues (pT) are shown in bold.

not shown). To check whether hyperphosphorylation could affect the function of LocZ, we then constructed strain Sp235 (R6, *locZ*-T67E/T78E), expressing LocZ with phosphomimetic mutation T67E/T78E at its own locus under the control of its native promoter. Again, phenotypic analysis did not reveal any differences between the *locZ* phosphomimetic mutant and the WT strain (data not shown).

DISCUSSION

Here, we report the identification and the characterization of LocZ, a novel cell division protein that plays a role in proper septum placement in *S. pneumoniae*. Cells lacking LocZ are viable but display aberrant morphologies and cell division defects and generate minicells, about half of which are anucleate, which are reported for the first time in streptococci. Conversely, we did not observe anucleate normal-size cells, which have been noted in *S. pneumoniae* mutants impaired in chromosome segregation, such as *parB* or *smc* mutants (51), suggesting that in the absence of LocZ the minicells arise from defects in septum placement rather than from defects in nucleoid partitioning.

A remarkable aspect of the *locZ* null mutant is the irregular shape of the cells, with poles that often deviate from the long cell axis. Accordingly, in cells lacking LocZ, PG synthesis is generally associated with misplaced division septa (see Fig. S2A in the supplemental material), supporting the notion that, in the pneumococcus, both sites of PG synthesis, peripheral and septal, are consistently coupled with the Z-rings (33). Nevertheless, since cell wall biosynthesis is not significantly disturbed in the Δ*locZ* mutant, there are two possible explanations for the misshaping. First, the activity of the PG biosynthetic enzymes may be affected in the absence of LocZ. Second, a simple mechanistic explanation assumes that, as the Z-ring is not perpendicular to the long cell axis, the cell symmetry cannot be maintained, although the function of the PG biosynthetic machinery is not affected.

FtsZ and FtsA localization is disturbed in the absence of LocZ, and misplacement of the Z-ring seems to be the main cause of aberrant cell division observed in the *locZ* mutant. At the molecular level, Z-rings not only appear shifted from the cell center but are often tilted randomly, relative to the long and short cell axes. Despite these defects, Z-ring formation is not usually compromised, and most of the Δ*locZ* cells are able to divide and separate, as would be expected if the cell division septum were placed randomly.

The mechanisms that regulate the division site selection have not been yet elucidated in *S. pneumoniae*. So far, the D,D-carboxypeptidase DacA/PBP3 is the only determinant proposed to be involved in the selection of the division site in pneumococci, on the basis that a *dacA* mutant is morphologically altered and exhibits severe division defects, with multiple septa initiated at aberrant locations (39, 52). Although some Δ*locZ* mutant cells may be rounder, as a result of the asymmetric septum placement, several important features distinguish the *locZ* from the *dacA* mutant phenotype. Multiple abortive initiation sites and regions with thickened cell wall reported for the *dacA* mutant are not seen in cells lacking LocZ, minicells are not a feature of the *dacA* mutant (39, 52), and DacA has been shown to localize preferentially on the surface of both cell hemispheres (39, 53). Our data show that LocZ localizes early at the division site, where it likely functions as a positive regulator of the Z-ring placement at midcell, although we do not know yet if it also promotes FtsZ polymerization. Since the Z-ring formation *per se* is not impaired in cells lacking LocZ and

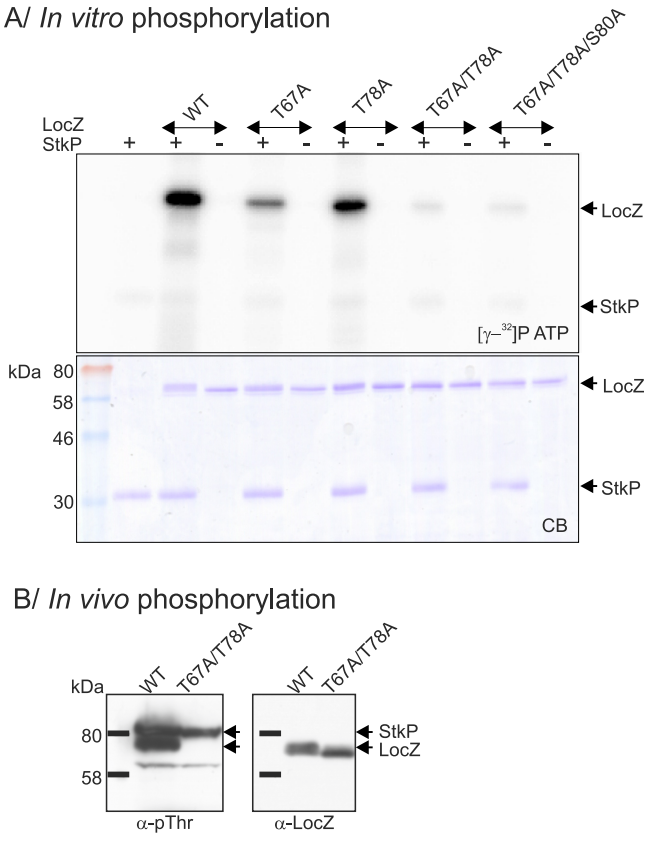

FIG 7 Phosphorylation of LocZ. (A) *In vitro* phosphorylation. WT and mutated derivatives of the recombinant His6-LocZ protein were subjected to phosphorylation by the recombinant StkP-kinase domain in the presence of [γ-^{32}P]ATP. Samples were resolved by SDS-PAGE, stained with Coomassie blue (CB), and exposed to a sensitive screen ([γ-^{32}P]ATP). The arrows on the right indicate positions of radioactively labeled proteins (upper panel) and Coomassie blue-stained proteins (lower panel). (B) *In vivo* phosphorylation. Phosphorylation of amino acids T67 and T78 was tested in whole-cell lysates of the WT (Sp208) and the mutant expressing unphosphorylatable LocZ-T67A/T78A (Sp234). Arrows indicate the positions of proteins. Note the difference in the LocZ migration, due to differential phosphorylation.

Z-rings are present in most of the cells, we cannot exclude the idea that LocZ affects only proper septum placement, thus acting solely as a spatial regulator of cell division.

Until now, no such molecular effectors were reported in pneumococci. The genome of streptococci does not encode homologues of the Min system (41) or any of the previously identified nucleoid occlusion effectors (34). Moreover, a mechanism involving nucleoid occlusion might be absent in *S. pneumoniae*, since it has been observed that FtsZ localizes over unsegregated nucleoids that completely separate concurrently with Z-ring constriction (54). Positive regulation of division site selection, through the SsgA/B system and PomZ, has been, so far, reported only in *Streptomyces* spp. and *M. xanthus*, respectively (29, 55). These positive regulators define the division site, recruit FtsZ, and promote its polymerization (29, 55), while the negative regulators, such as the Min and the MipZ/ParB systems, localize to the cell poles, preventing Z-ring formation at noncentral sites by inhibiting FtsZ polymerization (23, 28, 56, 57).

We show here that FtsZ is not properly localized at midcell in the absence of LocZ. Consistently, also other cell division proteins, such as FtsA, StkP, and DivIVA, which arrive at midcell together or after FtsZ (36, 38, 41), are also mislocalized in the Δ*locZ* mutant, reflecting the atypical position of the Z-ring in these cells and suggesting that their localization is, directly or indirectly, dependent on FtsZ. This may be particularly important for DivIVA, which localizes at the midcell but also at cell poles (41). Lenarcic et al. (58) reported that DivIVA is likely targeted to the septum and then to the cell poles due to an interaction with the concave membranes. Here, we observed DivIVA enrichment also on the deviated poles of the mutant cells and its delocalization in some misshapen, often round, cells, where it formed clusters at random positions (see Fig. S4 in the supplemental material), possibly due to the absence of prolate cell poles.

Both LocZ and DivIVA are substrates phosphorylated, *in vitro* and *in vivo*, by the single Ser/Thr protein kinase StkP (42, 59), which we have recently shown to control cell division in *S. pneumoniae* (38). Here, we identified two threonine residues, T67 and T78, in LocZ that are phosphorylated by StkP. However, when, to define the role of LocZ phosphorylation, we expressed the corresponding phosphoablative allele (LocZ-T67A/T78A) or the phosphomimetic allele (LocZ-T67E/T78E), both mutants showed a WT phenotype, suggesting that phosphorylation may not be crucial for LocZ function in cell division.

Consistent with the proposed function, LocZ is the first protein that localizes to midcell. Its position seems to associate with the "wall bands" or "equatorial rings," the markers for cell division in streptococci (30, 33, 35, 60), which are also shifted in the absence of LocZ. Considering our colocalization studies (Fig. 5), we propose a model for LocZ function. At the first stage of cell division, corresponding to the initial inward growth of the incipient septum at the cell equator, i.e., at the largest cell diameter, LocZ colocalizes with FtsZ and the other FtsZ-associated proteins, such as FtsA and StkP. Soon after the original equatorial ring splits and two wall bands are formed, LocZ associates with them, forming a characteristic doublet that is pushed away from the center, as the result of PG inserted in between the newly generated rings. As division progresses, and FtsZ constriction becomes evident at midcell, LocZ approaches the equators of the future daughter cells, directing FtsZ localization for the next division.

It was previously suggested that the equatorial ring alone could serve as the marker for septum placement, through a yet-unidentified mechanism (8, 60). Here, we hypothesize that LocZ may function as a molecular marker associated with the equatorial ring, spatially regulating Z-ring formation at the midcell. LocZ is a unique protein, conserved only in a closely phylogenetically related group of bacteria, such as streptococci, lactococci, and enterococci, suggesting that they evolved a highly specific solution to select their cell division site, reflecting the specific requirements of the group to maintain cell symmetry and shape.

MATERIALS AND METHODS

Bacterial strains, plasmids, and growth conditions. Bacterial strains and plasmids used in this study are listed in Table S2 in the supplemental material. *S. pneumoniae* Rx1, R6, and D39, well-characterized WT strains (38), were used throughout this study. All strains and their corresponding derivative mutants were grown statically at 37°C in Trypticase soy broth (TSB) or semi-synthetic C medium (61) supplemented with 0.1% yeast extract (C+Y). Blood agar plates were made from Columbia agar containing 5% defibrinated sheep blood. *S. pneumoniae* cells competent for transformation were obtained by the addition of the competence-inducing peptide CSP-1 (62). Medium composition and strain construction are detailed in Text S1 in the supplemental material. *Escherichia coli* DH5α, grown in Luria-Bertani (LB) broth at 37°C with shaking, was used as a general-purpose cloning host. When necessary, the following antibiotics were added at the indicated concentrations ($\mu g \cdot ml^{-1}$): erythromycin (Erm), 0.05; chloramphenicol (Cm), 10; kanamycin (Kan), 500; streptomycin (Str), 500; tetracycline (Tet), 2.5 or 1 (for *S. pneumoniae*); ampicillin (Amp), 100; spectinomycin (Sm) (100) (for *E. coli*).

Oligonucleotides, recombinant DNA and protein techniques, Western blotting, and mass spectrometry. Mutant constructions, recombinant DNA and protein techniques, Western blotting, and mass spectrometry analysis were performed as described in Text S1 in the supplemental material. Oligonucleotides are listed in Table S3 in the supplemental material. N-terminal and C-terminal protein fusions are designated TAG-Protein or Protein-TAG, respectively, throughout this study.

Environmental stress tolerance. Tolerance of pneumococcal strains to environmental stress was examined similarly as previously described (44). The Rx1 WT strain and its isogenic Δ*locZ* mutant were inoculated (6.8×10^6 CFU ml^{-1}) in TSB medium, and growth and viability were monitored turbidimetrically, by measuring optical density at 600 nm (OD_{600}) every 30 min and by counting viable cells onto agar plates, respectively (41). To investigate sensitivity to heat stress, cultures were inoculated into TSB medium prewarmed to 37°C and 40°C. Acid tolerance was monitored by measuring growth in TSB medium adjusted to pH 6.5 and 7.5. Alkaline tolerance was monitored at pH 8.0. To test the tolerance of the WT and the Δ*locZ* mutant to osmotic stress, bacteria were first grown to early exponential phase (OD_{600}, 0.2) and then inoculated into prewarmed TSB medium with or without 400 mM NaCl. The sensitivity to H_2O_2 was tested by exposing early exponential cultures (OD_{600}, 0.2) to 10 mM H_2O_2 for 15 min. Viable cell counts were determined by plating serial dilutions of cultures onto agar plates before and after exposure to H_2O_2.

Microscopy. For phase-contrast and DAPI staining analysis, cells were prepared as described previously (37). Bacterial cultures, grown to an OD_{600} of 0.3 in TSB, were fixed with 2.5% (vol/vol) paraformaldehyde, 0.03% glutaraldehyde, 30 mM sodium phosphate (pH 7.5), for 15 min at room temperature and 45 min on ice; washed two times in phosphate-buffered saline (PBS); and resuspended in GTE buffer (50 mM glucose, 20 mM Tris-HCl, pH 7.5, 10 mM EDTA) and fresh lysozyme solution (final concentration of 0.1 $mg \cdot ml^{-1}$). Cells were then transferred onto poly-L-lysine-coated PolyPrep slides (Sigma), washed twice with PBS, air dried, dipped in methanol at −20°C for 5 min, and allowed to air dry again. After rehydration, 2 μl Vectashield (Vector Laboratories) containing DAPI (1.5 $\mu g\ ml^{-1}$) was added and samples were examined using an Olympus Cell^R IX 81 microscope.

For transmission electron microscopy, exponentially growing bacterial cultures (20 ml) were centrifuged at 9,000 × *g* for 10 min and the cell pellets were resuspended in 10 ml of fresh medium. Fixation was performed according to the method in reference 63. Bacteria were prefixed in 0.1% OsO_4 for 1 h and then fixed overnight in 1% OsO_4. The fixed and extensively washed samples were dehydrated through an alcohol series followed by embedding into Vestopal resin. Ultrathin sections were contrasted using uranyl acetate and lead citrate (64). Final samples were viewed in a Philips CM100 electron microscope (FEI, formerly Philips EO, the Netherlands) at 80 kV. Digital images were recorded using a MegaViewII slow-scan camera at a magnification of ×46,000 and processed with the Analysis 3.2 software (Olympus Soft Imaging Solutions GmbH, Muenster, Germany) using standard modules.

For scanning electron microscopy, samples were processed in parallel with those for TEM. One milliliter of culture was prefixed with 1.5% glutaraldehyde for 1 h. Then, cells were washed with cacodylate buffer and fixed with 3% glutaraldehyde in cacodylate buffer overnight at 4°C. After fixation, cells were extensively washed and then allowed to sediment overnight onto poly-L-lysine-treated SPI pore filters (pore size of 0.2 μm) at 4°C. The filters were dehydrated through an alcohol series followed by absolute acetone and critical point dried from liquid CO_2 in a Balzers CPD 010 unit. The dried samples were sputter coated with gold in a Polaron sputter coater (E5100) (Quorum Technologies Ltd., Ringmer, United Kingdom) and finally examined in a Tescan Vega LSU scanning electron microscope (Tescan. Brno, Czech Republic) at 20 kV in secondary electron mode.

VanFL (Molecular Probes) staining of living cells was performed as described previously (38). Cells were grown to an OD_{600} of 0.2 in TSB and then labeled with 0.1 μg ml^{-1} of VanFL-vancomycin (50:50 mixture) for 5 min at 37°C, before examination by fluorescence microscopy.

Localization of fluorescently tagged protein was performed basically as described elsewhere (38). Cells expressing GFP or RFP fusion proteins under the control of the inducible P_{czcD} promoter were cultivated at 37°C in either TSB or C+Y medium, and expression was induced by the addition of $ZnCl_2$ to a final concentration of 0.45 mM for TSB medium or 0.15 mM for C+Y medium, respectively. Two microliters of culture was spotted onto the microscope slide and covered with 1% PBS or a C+Y agarose slab. Images were taken with an Olympus Cell^R IX 81 microscope equipped with an 100× oil immersion objective (numerical aperture [NA], 1.3) and an Olympus FV2T Digital B/W Fireware camera. Images were elaborated using the Cell^R version 2.0 software and CorelDRAW X3 (Corel Corporation). Fluorescence signals from protein colocalization analysis were analyzed by FluoView software (Olympus). The expression levels of CFP-FtsZ, GFP-FtsA, and GFP-StkP fusion proteins were about ~2-fold higher than those of their respective native counterparts (see Fig. S4E in the supplemental material) and did not affect the morphology of the cells or their localization, as previously reported (38, 48). Finally, time-lapse microscopy was carried out according to the method in reference 38. Briefly, cells were grown at 37°C in C+Y medium and attached to a thin 1.5% low-melting-point agarose C+Y matrix. The microscope slide was incubated at 37°C in a temperature-controlled chamber of the Olympus Cell^R IX 81 microscope. Phase-contrast and fluorescence images were taken every 10 min. The movies were assembled using ImageJ software.

Image analysis. Cell size was measured by automated MicrobeTracker software (45) using phase-contrast images from at least two microscopic fields from two independent experiments. The cell length of 400 cells was analyzed by statistical program GraphPad Prism 3.0. Fluorescence images of live dividing pneumococcal cells were manually binned into six division stages (36, 37, 41) based on cell morphology and localization profile. More than 300 cells were analyzed from at least two fields from each of two independent biological replicate experiments, and percentages of cells for each stage are indicated. Fluorescence intensity profiles showing distributions of molecules along the longitudinal cell axis were traced for representative cells in each division stage.

SUPPLEMENTAL MATERIAL

Supplemental material for this article may be found at http://mbio.asm.org/lookup/suppl/doi:10.1128/mBio.01700-14/-/DCSupplemental.

Figure S1, PDF file, 0.1 MB.
Figure S2, PDF file, 1.3 MB.
Figure S3, PDF file, 0.9 MB.
Figure S4, PDF file, 2.9 MB.
Movie S1, AVI file, 0.2 MB.
Movie S2, AVI file, 0.2 MB.
Text S1, PDF file, 0.2 MB.
Table S1, PDF file, 0.1 MB.
Table S2, PDF file, 0.1 MB.
Table S3, PDF file, 0.1 MB.

ADDENDUM IN PROOF

While this paper was under the last stage of review, Fleurie et al. published in Nature online (http://www.nature.com/nature/journal/v516/n7530/full/nature13966.html) that Spr0334, which they have named MapZ, is required for proper FtsZ localization in *Streptococcus pneumoniae* (A. Fleurie, C. Lesterlin, S. Manuse, C. Zhao, C. Cluzel, J. P. Lavergne, M. Franz-Wachtel, B. Macek, C. Combet, E. Kuru, M. S. VanNieuwenhze, Y. V. Brun, D. Sherratt, and C. Grangeasse, Nature **516:**259–262, 2014) and their findings are, overall, consistent with the main conclusions described here.

ACKNOWLEDGMENTS

This work was supported by the Czech Science Foundation (projects P302/12/0256 and P207/12/1568 to P.B.), by Institutional Research Concept grant RVO 61388971, and by grants from the National Research Agency (ANR-09-MIEN-004) and the ATIP/AVENIR Program for V.M.

We thank Sergio R. Filipe for the gift of plasmid pBCSMH036 and Marco Oggioni for providing us with strain R6. We thank Michael B. Whalen and Waldemar Vollmer for critical reading of the manuscript and valuable suggestions. We thank I. Zanella-Cléon from the Mass Spectrometry Unit (CCMP), UMS3444/US8 Biosciences Gerland Lyon Sud, France, for her technical assistance.

REFERENCES

1. **Bi EF, Lutkenhaus J.** 1991. FtsZ ring structure associated with division in *Escherichia coli*. Nature **354:**161–164. http://dx.doi.org/10.1038/354161a0.
2. **Trueba FJ.** 1982. On the precision and accuracy achieved by *Escherichia coli* cells at fission about their middle. Arch Microbiol **131:**55–59. http://dx.doi.org/10.1007/BF00451499.
3. **de Boer PA.** 2010. Advances in understanding *E. coli* cell fission. Curr Opin Microbiol **13:**730–737. http://dx.doi.org/10.1016/j.mib.2010.09.015.
4. **Egan AJ, Vollmer W.** 2013. The physiology of bacterial cell division. Ann N Y Acad Sci **1277:**8–28. http://dx.doi.org/10.1111/j.1749-6632.2012.06818.x.
5. **Lutkenhaus J, Pichoff S, Du S.** 2012. Bacterial cytokinesis: from Z ring to divisome. Cytoskeleton (Hoboken) **69:**778–790. http://dx.doi.org/10.1002/cm.21054.
6. **Rico AI, Krupka M, Vicente M.** 2013. In the beginning, *Escherichia coli* assembled the proto-ring: an initial phase of division. J Biol Chem **288:**20830–20836. http://dx.doi.org/10.1074/jbc.R113.479519.
7. **Margolin W.** 2005. FtsZ and the division of prokaryotic cells and organelles. Nat Rev Mol Cell Biol **6:**862–871. http://dx.doi.org/10.1038/nrm1745.
8. **Monahan LG, Liew AT, Bottomley AL, Harry EJ.** 2014. Division site positioning in bacteria: one size does not fit all. Front Microbiol **5:**19. http://dx.doi.org/10.3389/fmicb.2014.00019.
9. **Barák I, Wilkinson AJ.** 2007. Division site recognition in *Escherichia coli* and *Bacillus subtilis*. FEMS Microbiol Rev **31:**311–326. http://dx.doi.org/10.1111/j.1574-6976.2007.00067.x.
10. **Harry EJ.** 2001. Bacterial cell division: regulating Z-ring formation. Mol Microbiol **40:**795–803. http://dx.doi.org/10.1046/j.1365-2958.2001.02370.x.
11. **Margolin W.** 2001. Spatial regulation of cytokinesis in bacteria. Curr Opin

Microbiol **4:**647–652. http://dx.doi.org/10.1016/S1369-5274(01)00264-8.
12. **Bernhardt TG, de Boer PA.** 2005. SlmA, a nucleoid-associated, FtsZ binding protein required for blocking septal ring assembly over chromosomes in *E. coli*. Mol Cell **18:**555–564. http://dx.doi.org/10.1016/j.molcel.2005.04.012.
13. **Cho H, McManus HR, Dove SL, Bernhardt TG.** 2011. Nucleoid occlusion factor SlmA is a DNA-activated FtsZ polymerization antagonist. Proc Natl Acad Sci U S A **108:**3773–3778. http://dx.doi.org/10.1073/pnas.1018674108.
14. **Tonthat NK, Arold ST, Pickering BF, Van Dyke MW, Liang S, Lu Y, Beuria TK, Margolin W, Schumacher MA.** 2011. Molecular mechanism by which the nucleoid occlusion factor, SlmA, keeps cytokinesis in check. EMBO J **30:**154–164. http://dx.doi.org/10.1038/emboj.2010.288.
15. **Tonthat NK, Milam SL, Chinnam N, Whitfill T, Margolin W, Schumacher MA.** 2013. SlmA forms a higher-order structure on DNA that inhibits cytokinetic Z-ring formation over the nucleoid. Proc Natl Acad Sci U S A **110:**10586–10591. http://dx.doi.org/10.1073/pnas.1221036110.
16. **Wu LJ, Errington J.** 2004. Coordination of cell division and chromosome segregation by a nucleoid occlusion protein in *Bacillus subtilis*. Cell **117:**915–925. http://dx.doi.org/10.1016/j.cell.2004.06.002.
17. **Wu LJ, Ishikawa S, Kawai Y, Oshima T, Ogasawara N, Errington J.** 2009. Noc protein binds to specific DNA sequences to coordinate cell division with chromosome segregation. EMBO J **28:**1940–1952. http://dx.doi.org/10.1038/emboj.2009.144.
18. **Wu LJ, Errington J.** 2012. Nucleoid occlusion and bacterial cell division. Nat Rev Microbiol **10:**8–12. http://dx.doi.org/10.1038/nrmicro2671.
19. **de Boer PA, Crossley RE, Rothfield LI.** 1988. Isolation and properties of *minB*, a complex genetic locus involved in correct placement of the division site in *Escherichia coli*. J Bacteriol **170:**2106–2112.
20. **de Boer PA, Crossley RE, Rothfield LI.** 1989. A division inhibitor and a topological specificity factor coded for by the minicell locus determine proper placement of the division septum in *E. coli*. Cell **56:**641–649. http://dx.doi.org/10.1016/0092-8674(89)90586-2.
21. **de Boer PA, Crossley RE, Rothfield LI.** 1992. Roles of MinC and MinD in the site-specific septation block mediated by the MinCDE system of *Escherichia coli*. J Bacteriol **174:**63–70.
22. **Lee S, Price CW.** 1993. The *minCD* locus of *Bacillus subtilis* lacks the *minE* determinant that provides topological specificity to cell division. Mol Microbiol **7:**601–610. http://dx.doi.org/10.1111/j.1365-2958.1993.tb01151.x.
23. **Hu Z, Mukherjee A, Pichoff S, Lutkenhaus J.** 1999. The MinC component of the division site selection system in *Escherichia coli* interacts with FtsZ to prevent polymerization. Proc Natl Acad Sci U S A **96:**14819–14824. http://dx.doi.org/10.1073/pnas.96.26.14819.
24. **Pichoff S, Lutkenhaus J.** 2001. *Escherichia coli* division inhibitor MinCD blocks septation by preventing Z-ring formation. J Bacteriol **183:**6630–6635. http://dx.doi.org/10.1128/JB.183.22.6630-6635.2001.
25. **Adler HI, Fisher WD, Cohen A, Hardigree AA.** 1967. Miniature *Escherichia coli* cells deficient in DNA. Proc Natl Acad Sci U S A **57:**321–326. http://dx.doi.org/10.1073/pnas.57.2.321.
26. **Reeve JN, Mendelson NH, Coyne SI, Hallock LL, Cole RM.** 1973. Minicells of *Bacillus subtilis*. J Bacteriol **114:**860–873.
27. **Harry E, Monahan L, Thompson L.** 2006. Bacterial cell division: the mechanism and its precision. Int Rev Cytol **253:**27–94. http://dx.doi.org/10.1016/S0074-7696(06)53002-5.
28. **Thanbichler M, Shapiro L.** 2006. MipZ, a spatial regulator coordinating chromosome segregation with cell division in *Caulobacter*. Cell **126:**147–162. http://dx.doi.org/10.1016/j.cell.2006.05.038.
29. **Treuner-Lange A, Aguiluz K, van der Does C, Harms A, Gomez-Santos N, Schumacher D, Lenz P, Hoppert M, Kahnt J, Munoz-Dorado J, Sogaard-Andersen L.** 2013. PomZ, a ParA-like protein, regulates Z-ring formation and cell division in *Myxococcus xanthus*. Mol Microbiol **87:**235–253. http://dx.doi.org/10.1111/mmi.12094.
30. **Higgins ML, Shockman GD.** 1970. Model for cell wall growth of *Streptococcus faecalis*. J Bacteriol **101:**643–648.
31. **Higgins ML, Shockman GD.** 1976. Study of cycle of cell wall assembly in *Streptococcus faecalis* by three-dimensional reconstructions of thin sections of cells. J Bacteriol **127:**1346–1358.
32. **Tomasz A.** 2000. *Streptococcus pneumoniae*: functional anatomy, p 9–21. *In* Tomasz A (ed), *Streptococcus pneumoniae*: molecular biology and mechanisms of disease. Mary Ann Liebert Publishing, New York, NY.
33. **Massidda O, Nováková L, Vollmer W.** 2013. From models to pathogens: how much have we learned about *Streptococcus pneumoniae* cell division? Environ Microbiol **15:**3133–3157. http://dx.doi.org/10.1111/1462-2920.12189.
34. **Pinho MG, Kjos M, Veening JW.** 2013. How to get (a)round: mechanisms controlling growth and division of coccoid bacteria. Nat Rev Microbiol **11:**601–614. http://dx.doi.org/10.1038/nrmicro3088.
35. **Wheeler R, Mesnage S, Boneca IG, Hobbs JK, Foster SJ.** 2011. Super-resolution microscopy reveals cell wall dynamics and peptidoglycan architecture in ovococcal bacteria. Mol Microbiol **82:**1096–1109. http://dx.doi.org/10.1111/j.1365-2958.2011.07871.x.
36. **Lara B, Rico AI, Petruzzelli S, Santona A, Dumas J, Biton J, Vicente M, Mingorance J, Massidda O.** 2005. Cell division in cocci: localization and properties of the *Streptococcus pneumoniae* FtsA protein. Mol Microbiol **55:**699–711. http://dx.doi.org/10.1111/j.1365-2958.2004.04432.x.
37. **Morlot C, Zapun A, Dideberg O, Vernet T.** 2003. Growth and division of *Streptococcus pneumoniae*: localization of the high molecular weight penicillin-binding proteins during the cell cycle. Mol Microbiol **50:**845–855. http://dx.doi.org/10.1046/j.1365-2958.2003.03767.x.
38. **Beilharz K, Nováková L, Fadda D, Branny P, Massidda O, Veening JW.** 2012. Control of cell division in *Streptococcus pneumoniae* by the conserved Ser/Thr protein kinase StkP. Proc Natl Acad Sci U S A **109:**E905–E913. http://dx.doi.org/10.1073/pnas.1119172109.
39. **Morlot C, Noirclerc-Savoye M, Zapun A, Dideberg O, Vernet T.** 2004. The D,D-carboxypeptidase PBP3 organizes the division process of *Streptococcus pneumoniae*. Mol Microbiol **51:**1641–1648. http://dx.doi.org/10.1046/j.1365-2958.2003.03953.x.
40. **Noirclerc-Savoye M, Le Gouëllec A, Morlot C, Dideberg O, Vernet T, Zapun A.** 2005. In vitro reconstitution of a trimeric complex of DivIB, DivIC and FtsL, and their transient co-localization at the division site in *Streptococcus pneumoniae*. Mol Microbiol **55:**413–424. http://dx.doi.org/10.1111/j.1365-2958.2004.04408.x.
41. **Fadda D, Santona A, D'Ulisse V, Ghelardini P, Ennas MG, Whalen MB, Massidda O.** 2007. *Streptococcus pneumoniae* DivIVA: localization and interactions in a MinCD-free context. J Bacteriol **189:**1288–1298. http://dx.doi.org/10.1128/JB.01168-06.
42. **Nováková L, Bezousková S, Pompach P, Spidlová P, Sasková L, Weiser J, Branny P.** 2010. Identification of multiple substrates of the StkP Ser/Thr protein kinase in *Streptococcus pneumoniae*. J Bacteriol **192:**3629–3638. http://dx.doi.org/10.1128/JB.01564-09.
43. **Weng L, Biswas I, Morrison DA.** 2009. A self-deleting Cre-*lox-ermAM* cassette, Cheshire, for marker-less gene deletion in *Streptococcus pneumoniae*. J Microbiol Methods **79:**353–357. http://dx.doi.org/10.1016/j.mimet.2009.10.007.
44. **Sasková L, Nováková L, Basler M, Branny P.** 2007. Eukaryotic-type serine/threonine protein kinase StkP is a global regulator of gene expression in *Streptococcus pneumoniae*. J Bacteriol **189:**4168–4179. http://dx.doi.org/10.1128/JB.01616-06.
45. **Sliusarenko O, Heinritz J, Emonet T, Jacobs-Wagner C.** 2011. High-throughput, subpixel precision analysis of bacterial morphogenesis and intracellular spatio-temporal dynamics. Mol Microbiol **80:**612–627. http://dx.doi.org/10.1111/j.1365-2958.2011.07579.x.
46. **Daniel RA, Errington J.** 2003. Control of cell morphogenesis in bacteria: two distinct ways to make a rod-shaped cell. Cell **113:**767–776. http://dx.doi.org/10.1016/S0092-8674(03)00421-5.
47. **Eberhardt A, Wu LJ, Errington J, Vollmer W, Veening JW.** 2009. Cellular localization of choline-utilization proteins in *Streptococcus pneumoniae* using novel fluorescent reporter systems. Mol Microbiol **74:**395–408. http://dx.doi.org/10.1111/j.1365-2958.2009.06872.x.
48. **Henriques MX, Catalão MJ, Figueiredo J, Gomes JP, Filipe SR.** 2013. Construction of improved tools for protein localization studies in *Streptococcus pneumoniae*. PLoS One **8:**e55049. http://dx.doi.org/10.1371/journal.pone.0055049.
49. **Molle V, Leiba J, Zanella-Cléon I, Becchi M, Kremer L.** 2010. An improved method to unravel phosphoacceptors in Ser/Thr protein kinase-phosphorylated substrates. Proteomics **10:**3910–3915. http://dx.doi.org/10.1002/pmic.201000316.
50. **Sun X, Ge F, Xiao CL, Yin XF, Ge R, Zhang LH, He QY.** 2010. Phosphoproteomic analysis reveals the multiple roles of phosphorylation in pathogenic bacterium *Streptococcus pneumoniae*. J Proteome Res **9:**275–282. http://dx.doi.org/10.1021/pr900612v.
51. **Minnen A, Attaiech L, Thon M, Gruber S, Veening JW.** 2011. SMC is recruited to *oriC* by ParB and promotes chromosome segregation in *Strep-*

tococcus pneumoniae. Mol Microbiol **81:**676–688. http://dx.doi.org/10.1111/j.1365-2958.2011.07722.x.

52. **Schuster C, Dobrinski B, Hakenbeck R.** 1990. Unusual septum formation in *Streptococcus pneumoniae* mutants with an alteration in the D,D-carboxypeptidase penicillin-binding protein 3. J Bacteriol **172:** 6499–6505.
53. **Barendt SM, Sham LT, Winkler ME.** 2011. Characterization of mutants deficient in the L,D-carboxypeptidase (DacB) and WalRK (VicRK) regulon, involved in peptidoglycan maturation of *Streptococcus pneumoniae* serotype 2 strain D39. J Bacteriol **193:**2290–2300. http://dx.doi.org/10.1128/JB.01555-10.
54. **Land AD, Tsui HC, Kocaoglu O, Vella SA, Shaw SL, Keen SK, Sham LT, Carlson EE, Winkler ME.** 2013. Requirement of essential Pbp2x and GpsB for septal ring closure in *Streptococcus pneumoniae* D39. Mol Microbiol **90:**939–955. http://dx.doi.org/10.1111/mmi.12408.
55. **Willemse J, Borst JW, de Wall WE, Bisseling T, van Wezel GP.** 2011. Positive control of cell division: FtsZ is recruited by SsgB during sporulation of Streptomyces. Genes Dev **25:**89–99. http://dx.doi.org/10.1101/gad.600211.
56. **Dajkovic A, Lan G, Sun SX, Wirtz D, Lutkenhaus J.** 2008. MinC spatially controls bacterial cytokinesis by antagonizing the scaffolding function of FtsZ. Curr Biol **18:**235–244. http://dx.doi.org/10.1016/j.cub.2008.01.042.
57. **Marston AL, Thomaides HB, Edwards DH, Sharpe ME, Errington J.** 1998. Polar localization of the MinD protein of *Bacillus subtilis* and its role in selection of the mid-cell division site. Genes Dev **12:**3419–3430. http://dx.doi.org/10.1101/gad.12.21.3419.
58. **Lenarcic R, Halbedel S, Visser L, Shaw M, Wu LJ, Errington J, Marenduzzo D, Hamoen LW.** 2009. Localisation of DivIVA by targeting to negatively curved membranes. EMBO J **28:**2272–2282. http://dx.doi.org/10.1038/emboj.2009.129.
59. **Fleurie A, Cluzel C, Guiral S, Freton C, Galisson F, Zanella-Cleon I, Di Guilmi AM, Grangeasse C.** 2012. Mutational dissection of the S/T-kinase StkP reveals crucial roles in cell division of *Streptococcus pneumoniae*. Mol Microbiol **83:**746–758. http://dx.doi.org/10.1111/j.1365-2958.2011.07962.x.
60. **Zapun A, Vernet T, Pinho MG.** 2008. The different shapes of cocci. FEMS Microbiol Rev **32:**345–360. http://dx.doi.org/10.1111/j.1574-6976.2007.00098.x.
61. **Lacks S, Hotchkiss RD.** 1960. A study of the genetic material determining an enzyme in *Pneumococcus*. Biochim Biophys Acta **39:**508–518. http://dx.doi.org/10.1016/0006-3002(60)90205-5.
62. **Claverys JP, Havarstein LS.** 2002. Extracellular-peptide control of competence for genetic transformation in *Streptococcus pneumoniae*. Front Biosci **7:**d1798–d1814. http://dx.doi.org/10.2741/claverys.
63. **Kellenberger E, Sechaud J, Ryter A.** 1959. Electron microscopical studies of phage multiplication. IV. The establishment of the DNA pool of vegetative phage and the maturation of phage particles. Virology **8:**478–498. http://dx.doi.org/10.1016/0042-6822(59)90050-9.
64. **Reynolds ES.** 1963. The use of lead citrate at high pH as an electron-opaque stain in electron microscopy. J Cell Biol **17:**208–212. http://dx.doi.org/10.1083/jcb.17.1.208.